Characterization of Pneumatic Artificial Muscle System in an Opposing Pair Configuration

T. F. Tang[1], S. H. Chong[1], M. H. Tan[1], C. Y. Chan[1], K. Sato[2]

[1]*Motion Control Research Laboratory, Faculty of Electrical Engineering, Universiti Teknikal Malaysia Melaka, Hang Tuah Jaya, 76100 Durian Tunggal, Melaka, Malaysia.*

[2]*Interdisciplinary Graduate School of Science and Engineering, Tokyo Institute of Technology, 4259 Nagatsuta, Midori-ku, Yokohama 226-8502, Japan.*

horng@utem.edu.my

***Abstract*— Pneumatic artificial muscle (PAM) is a pneumatic actuator that commonly used in the biomimetic robotic devices in rehabilitation applications due to its advantageous in high power-to-weight ratio and high degree of safety in use characteristics. Several techniques exist in the literature for the PAM system modeling, and these include theoretical modeling, phenomenological modeling and empirical modeling. This paper focuses on explaining the experimental setup of an opposing pair configuration of PAM system, and gives an analysis of the pneumatic muscle system dynamic in the theoretical modeling. The simulated dynamic model is compared with the actual PAM system for the validation in the open-loop step and sinusoidal positioning responses and pressures. It is concluded that the simulation result is verified and agreed with the actual system.**

***Index Terms*— Mathematical modeling; Classic control; Pneumatic artificial muscle; Opposing pair configuration.**

I. INTRODUCTION

Nowadays, the development of advanced technologies is involving the number of robotic and automation applications. Those applications have required an actuation system in driving the motion of the system. Pneumatic muscle actuator becomes highly demanded as an actuation system in the industrial applications and biomimetic robotic devices, especially in rehabilitation applications, due to its advantageous in high power-to-weight ratio and high degree of safety in use characteristics. One of the pneumatic muscle actuators that commonly used is called McKibben pneumatic artificial muscle (PAM) that generates a pulling force via pressurized air and contracts in the axial direction while expanding in the radial direction. PAM consists of an inflatable rubber tube sheathed by a braided mesh. It is a promising actuator in robotics since its driving force is large despite its light weight. Thus, PAM has attracted much attention in welfare devices due to its high safety, low weight and powerful output [1]. For example, it has been applied as a power assist device for rehabilitation applications [2-6]. However, PAM has significant nonlinearity, hysteresis and creep phenomenon. These limitations lead to a low controllability and a high difficulty in achieving the precision system control.

In practice, it is difficult to estimate correctly the model parameters which govern the dynamics of a PAM. In order to model the dynamics of PAM, several modeling methods have been studied, such as theoretical of mathematical modeling, phenomenological modeling and empirical modeling. Chou and Hannaford [7] derived a model based on the principle of virtual work argument of an infinitely thin inner tube and continuously cylindrical shape actuator. Tondu and Lopez [8] modeled the noncylinderical form of the PAM to improve the accuracy of model. Besides, Doumit et al. [9] presented a force-based static model by taking into account the netting analysis of the muscle braid, as well as the bladder effects. The result showed that the proposed force-based model is more accurate than the model that proposed by Chou and Hannaford.

These theoretical models limit its application for real-time control because it is too complex in structure and requires too many parameters that are difficult to obtain during experimentation. Therefore, some researchers have devoted to adopt the phenomenological model to describe the PAM's dynamics. Reynold et al. [10] introduced a model that used visco-elastic parameters to describe the behavior of PAM. This model consists of a parallel arrangement of a spring element, a damping element and a contractile force element. The authors claimed that the coefficient functions of the three-element model can be applied to the dynamic case. Furthermore, Li et al. [11] proposed a nonlinear dynamic model using the generated force of PAM to produce a function of the operating pressure and contraction length of the PAM. This model includes a viscous damping coefficient as well.

In this paper, the theoretical modeling of dynamic characteristics for the PAM system in opposing pair configuration is discussed. In order to validate the usefulness of the modeled dynamic PAM system in numerical, it is therefore compared with the experimental performances. This study contributes in the analysis of the overall system dynamics, and aims to understand the characteristics of the PAM system. The rest of this paper is organized as follows. In Section 2, the experimental setup of PAM system is presented. Section 3 describes the dynamic of the PAM system mathematically. Comparison between simulation and experimental result is discussed in Section 4 and followed by conclusion in Section 5.

II. Experimental Setup

An experimental setup is designed and constructed using two pneumatic artificial muscles (PAMs) and a mover is located in between the two PAMs in a horizontal motion, as shown in Figure 1. The two PAMs (FESTO DMSP-10-150N-RM-CM) generate pulling forces to push and pull the 2kg mover along the horizontal moving direction in a maximum working range of $\pm$4.5mm. Air is injected from the pressure supply with a pressure of 0.5MPa and controlled by a 5-port 3-way proportional servo valve (FESTO MPYE-5-1/8LF-010-B). The pressures in the two PAMs are measured using two pressure sensors (SMC PSE540A-01) with the resolution of 0.0012MPa, while the displacement of the mover is measured using a linear encoder with the resolution of 0.1µm. A data acquisition unit is used to interface with a host computer that installed MATLAB/Simulink software. The sampling time is 0.1ms.

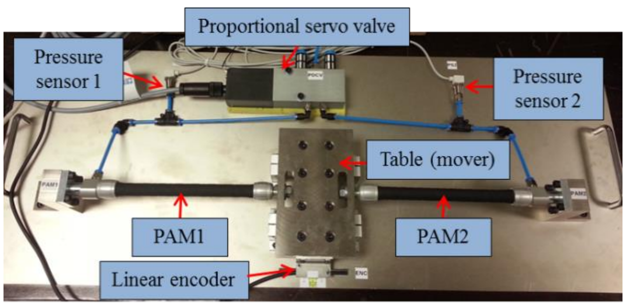

Figure 1: Overview of the PAM system (top view)

The PAM system is constructed in an opposing pair configuration. The initial position of the table (mover) is in the middle position, 0mm. The displacement of the table is considered as negative value when PAM1 contracts, and positive value when PAM2 contracts. The McKibben PAM consists of an inflatable rubber tube sheathed by a braided mesh. It has variable-stiffness spring-like characteristics due to its physical structure. Figure 2 shows the free body diagram of the PAM mechanisms.

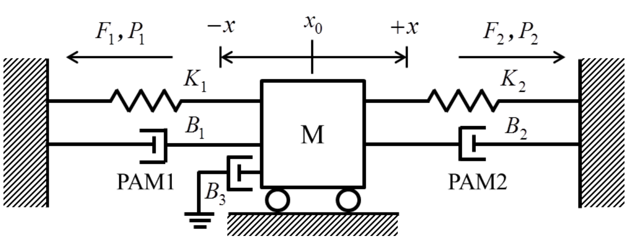

Figure 2: Free body diagram of the PAM mechanisms

III. Characteristic Modeling

In this section, the PAM system dynamic is discussed in sequence. In order to analysis the system dynamics, the mathematical modeling involves the consideration of the mass flow rates through the servo valve, the determination of the pressures, volumes and temperature of the air in the PAMs, the determination of the forces through PAMs, and the determination of the load dynamics. The overall dynamic model of the PAM system is formulated using the flow dynamics, G_ψ, mass flow dynamics, $G_{\dot{m}}$, pressure dynamics, $G_{\dot{P}}$, force dynamics, G_F, volume dynamics, G_V and motion equation, G_x. Figure 3 shows the block diagram of the overall system dynamic. Table 1 presented the system parameters and its numerical value.

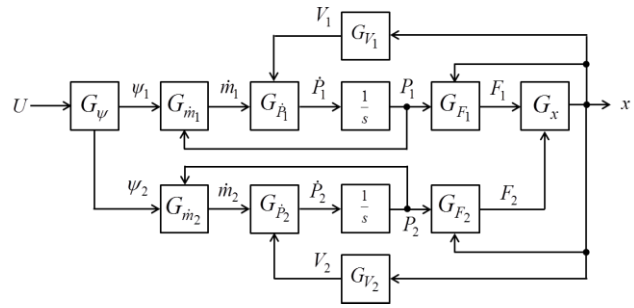

Figure 3: Block diagram of the overall system dynamic

Table 1: System parameters and numerical values

Parameter	Symbol	Numerical value
Air constant	$\bar{R}$	287J/kg.K
Atmospheric pressure	P_{atm}	3.8 x 10^3Pa
Change rate of pressure PAM1	$\dot{P}_1$	kg/ms^3
Change rate of pressure PAM2	$\dot{P}_2$	kg/ms^3
Critical pressure ratio	P_{cr}	0.528
Damping coefficient	B	1.8 x 10^3Ns/m
Displacement of the mover	x	m
Effective orifice area	A	6.28 x 10^{-7}m^2
Estimated coefficient	a_0	-12N
Estimated coefficient	a_1	3.5 x 10^{-3}m^2
Estimated coefficient	b_0	657.9N/m
Estimated coefficient	b_1	1.96 x 10^{-3}m
Estimated coefficient	b_2	-3 x 10^{-6}m^3/N
Flow function of PAM1	ψ_1	-
Flow function of PAM2	ψ_2	-
Force of PAM1	F_1	N
Force of PAM2	F_2	N
Friction coefficient	$F_{friction}$	2 x 10^4N/m
Initial PAM volume	V_0	4 x 10^{-6}m^3
Input signal	U	V
Mass flow rate of PAM1	$\dot{m}_1$	kg/s
Mass flow rate of PAM2	$\dot{m}_2$	kg/s
Mass of the mover	M	2.123kg
Maximum of flow function	ψ_{max}	-
Pressure of gas of PAM1	P_1	Pa
Pressure of gas of PAM2	P_2	Pa
Specific heat ratio	γ	1.4
Supply pressure	P_s	3.9 x 10^5Pa
Temperature of gas	T	293K
Volume flow rate of PAM1	Q_1	1 x 10^{-9}m^3/s
Volume flow rate of PAM2	Q_2	1 x 10^{-9}m^3/s
Volume of gas of PAM1	V_1	m^3
Volume of gas of PAM2	V_2	m^3
Volume rate of PAM	v	2 x 10^{-4}m^2

A. Mass Flow Dynamics

The motion of the mover is regulated by a servo valve that features a position-controlled spool. The spool position is controlled by the voltage signal from 0V to 10V, where the middle spool position is equivalent to 5V. In the modeling, the input signal, U is defined as the range of ± 5V, where the middle position is equivalent to 0V. In general, the mass flow rate is a function of velocity of the gas, the density of the gas, and the orifice area. However, the effective orifice area is governed by the control voltage of the servo valve in this case. Therefore, the mass flow dynamics, $G_{\dot{m}}$ of PAM1 and PAM2 are formulated in Equation (1) and Equation (2) respectively. The dynamics are assumed that gas behaves ideally, no heat exchange occurs, and temperature remains constant. The room temperature is considered as 20ºC.

$$\dot{m}_1 = -\sqrt{\frac{2}{\bar{R}T}}\psi_1 U \tag{1}$$

$$\dot{m}_2 = \sqrt{\frac{2}{\bar{R}T}}\psi_2 U \tag{2}$$

Besides, the flow dynamics, G_ψ is modeled into two conditions, which the PAM is in the condition of inflation or deflation as shown in Equation (3) and Equation (4).

$$\psi_1 = \begin{cases} \psi(P_1, P_{atm}) & if\ U \geq 0\ \text{(deflation)} \\ \psi(P_s, P_1) & if\ U < 0\ \text{(inflation)} \end{cases} \tag{3}$$

$$\psi_2 = \begin{cases} \psi(P_s, P_2) & if\ U \geq 0\ \text{(inflation)} \\ \psi(P_2, P_{atm}) & if\ U < 0\ \text{(deflation)} \end{cases} \tag{4}$$

where ψ_1 and ψ_2 have two conditions which are choked flow and subsonic flow as a function of the downstream to upstream pressure ratio. Equation (5) and Equation (6) show the flow function of PAM1 in deflation and inflation conditions, respectively, while the flow function of PAM2 in inflation and deflation conditions is shown in Equation (7) and Equation (8) respectively. Furthermore, ψ_{max} is presented in Equation (9).

$$\psi(P_1, P_{atm}) = \begin{cases} \psi_{max} P_1 & if\ \frac{P_{atm}}{P_1} \leq P_{cr}\ \text{(choked)} \\ \psi_{max} P_1 \sqrt{1 - \left(\frac{\frac{P_{atm}}{P_1} - P_{cr}}{1 - P_{cr}}\right)^2} & if\ \frac{P_{atm}}{P_1} > P_{cr}\ \text{(subsonic)} \end{cases} \tag{5}$$

$$\psi(P_s, P_1) = \begin{cases} \psi_{max} P_s & if\ \frac{P_1}{P_s} \leq P_{cr}\ \text{(choked)} \\ \psi_{max} P_s \sqrt{1 - \left(\frac{\frac{P_1}{P_s} - P_{cr}}{1 - P_{cr}}\right)^2} & if\ \frac{P_1}{P_s} > P_{cr}\ \text{(subsonic)} \end{cases} \tag{6}$$

$$\psi(P_s, P_2) = \begin{cases} \psi_{max} P_s & if\ \frac{P_2}{P_s} \leq P_{cr}\ \text{(choked)} \\ \psi_{max} P_s \sqrt{1 - \left(\frac{\frac{P_2}{P_s} - P_{cr}}{1 - P_{cr}}\right)^2} & if\ \frac{P_2}{P_s} > P_{cr}\ \text{(subsonic)} \end{cases} \tag{7}$$

$$\psi(P_2, P_{atm}) = \begin{cases} \psi_{max} P_2 & if\ \frac{P_{atm}}{P_2} \leq P_{cr}\ \text{(choked)} \\ \psi_{max} P_2 \sqrt{1 - \left(\frac{\frac{P_{atm}}{P_2} - P_{cr}}{1 - P_{cr}}\right)^2} & if\ \frac{P_{atm}}{P_2} > P_{cr}\ \text{(subsonic)} \end{cases} \tag{8}$$

$$\psi_{max} = \left(\frac{2}{\gamma + 1}\right)^{\frac{1}{\gamma - 1}} \sqrt{\frac{\gamma}{\gamma + 1}} \tag{9}$$

B. Motion Equation

During the contraction process, the PAM is expanding its diameter and reducing its length at the same time. Besides, the maximum force is generated at the beginning of the contraction, and the force decreases with the increment of the contraction. The motion equation of the PAM mechanism can be described as follows:

$$M\ddot{x} + B\dot{x} = F_2 - F_1 - F_{friction} \tag{10}$$

In order to validate the modeled dynamic of PAM system in numerical, it is therefore compared and verified with the experimental performances.

IV. Experiment Result

In this section, the comparison of open-loop responses are discussed between the simulation using the dynamic model as derived and experimental using the actual PAM system. The model parameters are identified based on the experimental results.

A. Static Relationships

The static relationships between input voltage, pressures of PAM1 and PAM2, and mover position are summarized. Figure 4 presents the static relationship between input voltage and pressure of PAM1 and PAM2; the static relationship between input voltage and displacement. The result shows that the system is high nonlinearities.

Based on Figure 4(a), the maximum pressure of the contracted PAM is about 390kPa rather than 500kPa (supply pressure), due to the losses caused by the friction inside the tubing and the leakage from the servo valve when the pressurized air transferred from the compressor to the PAM. Besides, the maximum pressure of the relaxed PAM is about 3.8kPa, which is lower than the atmospheric pressure as 101.3kPa. This is because the contracted PAM is pulling the relaxed PAM, which caused the pressure inside the relaxed PAM becomes lower than the atmospheric pressure. As a result, the supply pressure and atmospheric pressure are defined as 390kPa and 3.8kPa respectively for the simulation.

Furthermore, the pressure is 210kPa when the mover is at the middle position with the input voltage of 5.1V. The changes of pressure are large from 4.5V to 5.8V with the small changes of input voltage. However, the pressures from 0V to 3V and 7V to 10V have slight changes with respect to the large changes of input voltage. This happened because the relaxed PAM becomes stiff when it has been pulled over the elasticity limit.

The displacement of the mover is proportional to the pressure difference between PAM2 and PAM1. The result of the displacement is nonlinear between the contraction of the PAM1 and the PAM2 due to the hysteresis and the nonlinear friction force. The working range is around ±3.2mm for the 0.5MPa of supply pressure as shown in Figure 4(b).

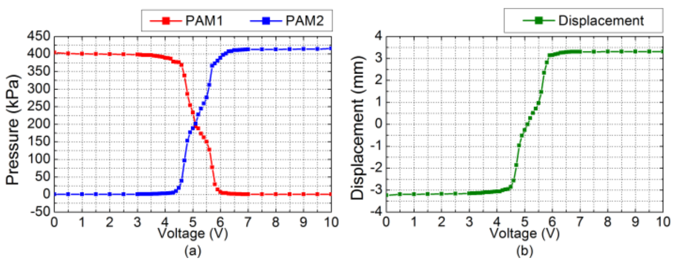

Figure 4: The static relationships between (a) input voltage and pressure of PAM1 and PAM2, and (b) input voltage and displacement

B. *Experimental Validation*

Figure 5 and Figure 6 show the open-loop step responses of the PAM system with the input signal of 1V and 3V respectively. In step response, the simulated pressure of PAM1, P_1 is similar to the experimental pressure as shown in Figure 5 and Figure 6. However, the simulated pressure of PAM2, P_2 is slightly different as compared to the experimental pressure in the inflation process for 1V and 3V, due to the nonlinear of friction force, air flow, and pressure supply from the compressor which cannot be modeled accurately in theoretical. As a result, the experimental displacement is slightly increasing after steady-state. Besides, the physical structure of the PAM also one of the factors that results in higher error of P_2 when comparing the performances of 1V and 3V. This is because the material of the PAM is made of rubber and the rubber cause the hysteresis. The experimental results in Figure 5 and Figure 6 demonstrate that a higher input voltage results in a higher pressure error in the contracted PAM. For the reason, a higher input voltage produces a higher initial velocity, thus a higher initial velocity is expanding the PAM more than a lower initial velocity as shown in Figure 5(d) and Figure 6(d). The pressure error is then caused the displacement error became larger as the input voltage increased.

Figure 7 and Figure 8 show the open-loop sinusoidal responses of the PAM system with the amplitude of 1V and 3V with frequency of 1Hz respectively. Based on the comparative sinusoidal performance in Figure 7 and Figure 8, the pressures and displacement of experiments are tracked in the responses by referring to the simulation results. However, the amplitudes are not achieved due to the unmodeled nonlinear characteristics in numerical analysis as well. Overall, it can be concluded that the simulation results are proven and agreed well with the experimental one.

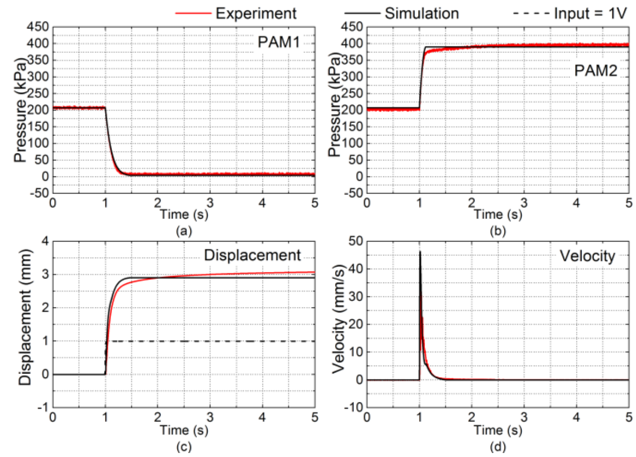

Figure 5: Open-loop step responses of (a) P_1, (b) P_2, (c) displacement and (d) velocity with the simulation and experimental results with the input signal of 1V

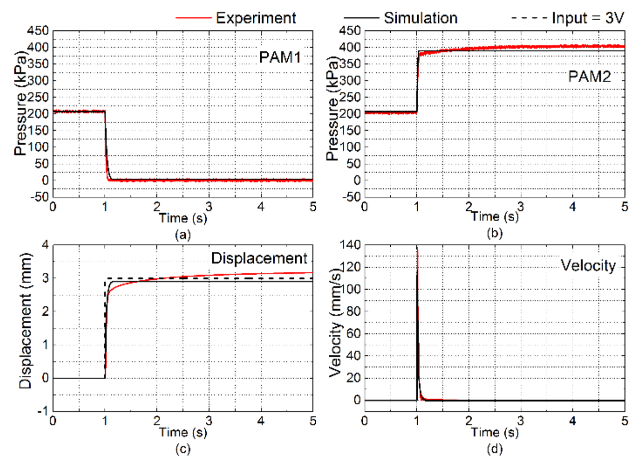

Figure 6: Open-loop step responses of (a) P_1, (b) P_2, (c) displacement and (d) velocity with the simulation and experimental results with the input signal of 3V

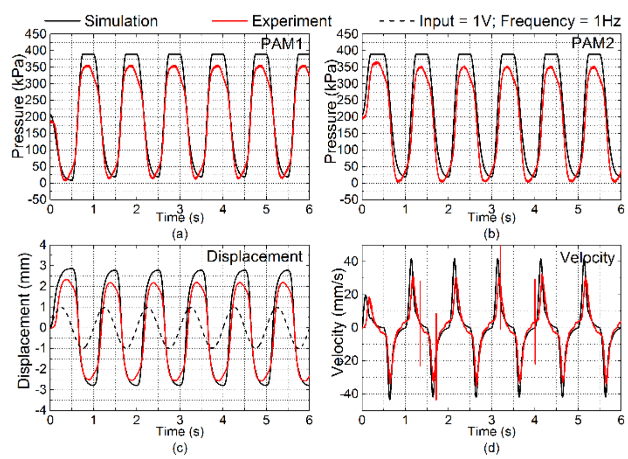

Figure 7: Open-loop sinusoidal responses of (a) P_1, (b) P_2, (c) displacement and (d) velocity with the simulation and experimental results with the amplitude of 1V and frequency of 1Hz

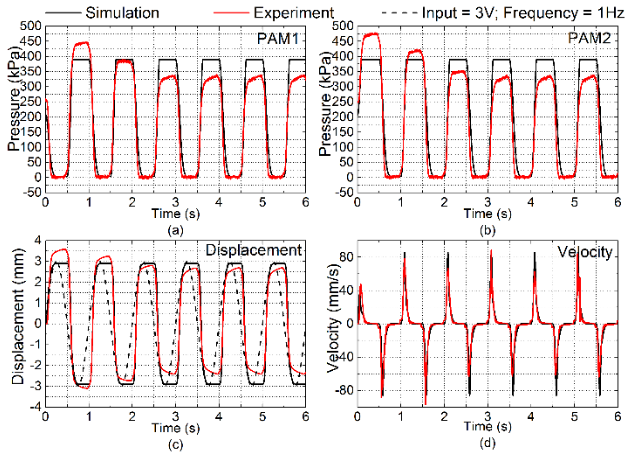

Figure 8: Open-loop sinusoidal responses of (a) P_1, (b) P_2, (c) displacement and (d) velocity with the simulation and experimental results with the amplitude of 3V and frequency of 1Hz

V. CONCLUSION

This paper presented the theoretical modeling of a highly nonlinear positioning system that work in a small travel range, ±3.2mm. Therefore, an opposing pair configuration of a PAM system was successfully constructed and the overall PAM system dynamics have been theoretically modeled. The characteristics of mass flow, pressure, force and motion of the PAM system was proved and explained. The static experiment has been done to model the relationship between the supply voltage with the table motion and working-pressure. The simulation result of dynamic model is macroscopically verified with the actual PAM system. The modeled dynamic is proven and agreed well with the experimental performance. The PAM system is a highly nonlinear system due to the PAM mechanism itself, friction force, air flow and the pressure supply from the compressor. It is difficult to identify a complex and the exact dynamic model by including all the nonlinear characteristics.

ACKNOWLEDGMENT

The authors would like to be obliged to Motion Control Research Laboratory, Faculty of Electrical Engineering, Universiti Teknikal Malaysia Melaka for providing the laboratory facilities and equipment support. This work is financially supported by the Fundamental Research Grant Project (FRGS/2/2014/TK03/FKE/02/F00240) and Center for Robotics and Industrial Automation (CeRIA), Faculty of Electrical Engineering, Universiti Teknikal Malaysia Melaka.

REFERENCES

[1] S. Wang, K. Sato, and T. Kagawa, "Precise positioning of pneumatic artificial muscle systems", *Journal of Flow Control, Measurement & Visualization*, 2014, 2:138-153.

[2] Z. Wong, C. Teng, and Y. Z. Chong, Power assisted pnumatic-based knee-ankle-foot-orthosis for rehabilitation. *IEEE-EMBS Conference on Biomedical Engineering and Sciences*, 2012, 300-304.

[3] S. Balasubramanian, J. Ward, T. Sugar, and J. He, "Characterization of the dynamic properties of pneumatic muscle actuators" *IEEE 10th International Conference on Rehabilitation Robotics*, 2007, 764-770.

[4] T. G. Sugar, Jiping He, E. J. Koeneman, J. B. Koeneman, R. Herman, H. Huang, R. S. Schultz, D. E. Herring, J. Wanberg, S. Balasubramanian, P. Swenson, and J. A. Ward, "Design and control of RUPERT: a device for robotic upper extremity repetitive therapy", *IEEE Transactions on Neural Systems and Rehabilitation Engineering*, 2007, 15(3):336-346.

[5] T. Noritsugu, M. Takaiwa, and D. Sasaki, "Pneumatic rubber artificial muscles and application to welfare robotics", *Next-Generation Actuators Leading Breakthroughs*, 2010, 255-266.

[6] S. Hussain, S. Q. Xie, and P. K. Jamwal, "Robust nonlinear control of an intrinsically compliant robotic gait training orthosis", *IEEE Transactions Systems, Man, Cybernetics: Systems*, 2013, 43(3):655-665.

[7] Ching-Ping Chou, and B. Hannaford, "Measurement and modeling of McKibben pneumatic artificial muscles", *IEEE Transactions on Robotics and Automation*, 1996, 12(1):90-102.

[8] B. Tondu, and P. Lopez, "Modeling and control of McKibben artificial muscle robot actuators", *IEEE Control Systems Magazine*, 2000, 20(2):15-38.

[9] M. Doumit, A. Fahim, and M. Munro, "Analytical modeling and experimental validation of the braided pneumatic muscle", *IEEE Transactions on Robotics*, 2009, 25(6):1282-1291.

[10] D. B. Reynolds, D. W. Repperger, C. A. Phillips, and G. Bandry, "Modeling the dynamic characteristics of pneumatic muscle", *Annals of Biomedical Engineering*, 2003, 31(3):310-317.

[11] H. Li, K. Kawashima, K. Tadano, S. Ganguly, and S. Nakano, "Achieving haptic perception in forceps manipulator using pneumatic artificial muscle", *IEEE/ASME Transactions on Mechatronics*, 2013, 18(1):74-85.

[12] V. Jouppila, S. Andrew Gadsden, and A. Ellman, "Experimental comparisons of sliding mode controlled pneumatic muscle and cylinder actuators", *Journal of Dynamic Systems, Measurement, and Control*, 2014, 136(4):044503-1-10.

[13] X. Shen, "Nonlinear model-based control of pneumatic artificial muscle servo systems", *Control Engineering Practice*, 2010, 18(3):311-317.

[14] S. Ganguly, A. Garg, A. Pasricha, and S. K. Dwivedy, "Control of pneumatic artificial muscle system through experimental modeling", *Mechatronics*, 2012, 22(8):1135-1147.